Soft Matter

Accepted Manuscript

This is an *Accepted Manuscript*, which has been through the Royal Society of Chemistry peer review process and has been accepted for publication.

Accepted Manuscripts are published online shortly after acceptance, before technical editing, formatting and proof reading. Using this free service, authors can make their results available to the community, in citable form, before we publish the edited article. We will replace this *Accepted Manuscript* with the edited and formatted *Advance Article* as soon as it is available.

You can find more information about *Accepted Manuscripts* in the Information for Authors.

Please note that technical editing may introduce minor changes to the text and/or graphics, which may alter content. The journal's standard Terms & Conditions and the Ethical guidelines still apply. In no event shall the Royal Society of Chemistry be held responsible for any errors or omissions in this *Accepted Manuscript* or any consequences arising from the use of any information it contains.

ROYAL SOCIETY OF CHEMISTRY

www.rsc.org/softmatter

Soft Matter

RSCPublishing

COMMUNICATION

Assessment of Micro-Polarity Anisotropy as a function of Surfactant Packing in sodium dodecyl sulphonate-Hexane Reverse Micelles

Cite this: DOI: 10.1039/xoxxoooooox

Received ooth January 2012,
Accepted ooth January 2012

DOI: 10.1039/xoxxoooooox

www.rsc.org/

Xin Peng[a b], Xing-Zhong Yuan[b], P. Somasundaran[c] and Partha Patra[c*]

The micro-polarity anisotropy behaviour across the aqueous phase of a SDS (sodium dodecyl sulphonate)-hexane reverse micelle (RM) rely on the SDS packing in the oil-water interfacial self-assembled surfactant structure of the RM.

Reverse micelle (RM) systems are advantageous for a number of processes such as nanoparticle synthesis[1] and liquid-liquid extraction of enzymes[2]. The effectiveness of these processes rely on the micro-polarity anisotropy (MPA) of the aqueous phase of a RM. The MPA of a RM is according to its water: surfactant (ω_0) ratio.[3] A reliable estimate of MPA is critical to predict and regulate enzyme activity in RMs.[4,5] The common approaches assess MPA($\vec{r}$) ($\vec{r}$ - the radial distance, Fig. 1) in terms of the microstructural characteristics of water in RMs[6] and the electrostatic potential distribution ($\psi(\vec{r})$) across the aqueous phase (Fig. 1b)[7,8]. Spectroscopy studies and molecular dynamic simulations reveal that, in terms of the micro-polarity attributes, the RM aqueous phase comprises at least two spatially separable regions (Fig. 1a and b), the interfacial region (ordered water) and the core region (bulk water).[9,6] The $\psi(\vec{r})$ profile that exemplifies MPA owe to the oil-water interfacial charge density levels (per volume of water in a RM) of the surfactant head groups, and, the distributional aspects of the counter ions in the aqueous phase. The $\psi(\vec{r})$ profiles exhibit an exponential form (Fig. 1b).[6-9] For the aqueous phases in the vicinity of the surfactant-stabilized oil-water interfaces, the ψ profile attributes to the surfactant chemistries. The ψ profile for these interfacial systems are developed as per the electrical double layer (EDL) models.[10-13] Conversely, as the volume of the confined (nano-sized) aqueous phase of a RM is much less, the EDL characteristics are governed by the interfacial charge density levels (per RM water content), which decrease as the ω_0 values are higher. The charge density level, even at a particular ω_0 value, could vary depending on the degree of surfactant packing (inter-surfactant distances) in the self-assembled surfactant structure (SASS) of a RM.[14] Thus, the EDL characteristics that determine the MPA attribute to the surfactant -types and -density/packing in a SASS.[7,8] We assessed the $MPA(\vec{r})$ as a function of surfactant density/packing in the SASSs for the SDS (sodium dodecyl sulphonate)-hexane RMs.[15]

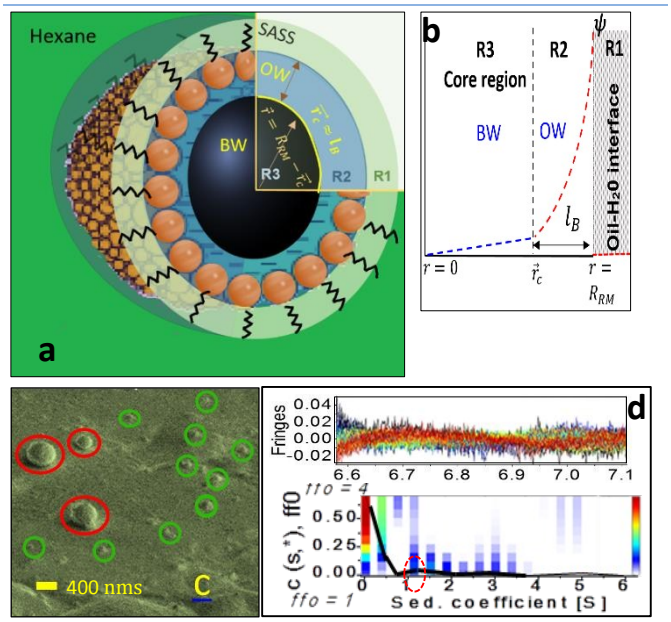

Fig. 1. (a) An illustration of the spatially segregated regions of a RM: SASS region (R1), interfacial region (R2), and the core (R3). A $\psi(\vec{r})$ profile is shown (b). A Cryo SEM image (c) shows small RMs of sizes < 50 nms (green circles); a few large RMs (red circles). AUC results (d) reveals the RMs as spherical (peak in red circle).R_{RM} and l_B are RM radius and Berrium length respectively.

The RMs were devised by adding desired amounts of water to SDS-hexane solutions (ESI 1). Cryo-SEM (ESI 2) images indicated that the RM sizes were < 50 nms ($\omega_0 \approx 24$; Fig. 1c). Analytical ultra-centrifuge (AUC) studies (ESI2) reveal the RMs as spherical in shape (Fig. 1d). The RMs with ω_0 in the range of 5 to 25 were spherical and of sizes in the range of 10 to 50 nms. For ESR studies (ESI 1), 16-DSA (16-DOXYL-stearic acid) probe having NȮ radical was added to the RM samples in desired amounts. The hyperfine splitting constant (a_N) - MPA($\vec{r}$), and the rotational correlation time (τ_c) -

Soft Matter Accepted Manuscript

surfactant packing in SASS, were estimated for these RM systems. The application of ESR technique is a reliable option as the energy absorbance value of a probe with free radical, which can locate in the aqueous and SASS regions, allows to concurrently estimate the MPA and SASS packing aspects. Microstructural aspects of RM water was studied using IR (Attenuated Total reflection-Infrared) spectroscopy (ESI 1).

We compartmentalize a RM's environment into three spatially segregated and sequentially placed regions (Fig. 1a and b), and the MPA ($\vec{r}$) of these regions were assessed in terms of their contribution to the RM's $\psi(\vec{r})$ profile. The non-linear Poisson Boltzmann description of the $\psi(\vec{r})$ profile that associates these three regions is:

$$\nabla\psi = \frac{1}{r^2}\frac{d}{dr}\left(r^2\frac{d\psi}{dr}\right) = -\frac{4\pi e}{\varepsilon}n(R)\exp-\frac{e\psi(r)}{kT} \quad \text{..... (1)}$$

A solution to Eqn. 1 would require the determination of at least two dimensionless variables: x=κr and ξ=κR$_{RM}$, where κ is the inverse of the Debye length, r the radial distance, and R$_{RM}$ the RM size. A numerical solution to these dimensionless variables can be found elsewhere.[10,19] A general form of $\psi(\vec{r})$ for a RM can be written as:

$$e\frac{\psi(r)}{kT} = f(x) - f(\xi) \quad \text{..... (2)},$$

$$f(x) = \frac{e}{kT}\left[\psi(\vec{r}) - \psi(0)\right] \quad \text{..... (3)},$$

where, $\left(\frac{df}{dx}\right)_{x=\xi} = -\frac{(1-\beta)L_B R}{\sigma\xi}$, $\left(\frac{df}{dx}\right)_{x=0} = 0$.

The ξ term is dependent on the association coefficient of the counter ions, given as β. [10,19] The parameters that allow to differentiate the $\psi(\vec{r})$ profile for the regions R2 and R3 are:

$\eta = \frac{(1-\beta)L_B}{2\sigma}$, $L_B = 4\pi l_B$, where, $l_B = Bjerrum\ length$

For R$_{RM} \leq l_B$, the ψ decreases in an exponential manner from the interface to the core, and a plateau region of the $\psi(\vec{r})$ profile is absent. For R$_{RM} >> l_B$, the plateau part of the $\psi(\vec{r})$ profile represents the $\vec{r} \approx 0$ - $(R_{RM} - l_B)$ region (R3). And, this plateau region changes minimally with increase in RM sizes, as the micro-polarity contributions owe to the bulk-type water therein. In order to gain insights into how the $\psi(\vec{r})$ profiles differentiate for the RMs of different sizes, the responses of the NȮ of 16-DSA in RMs of different sizes were determined. These responses were in terms of the energy absorbance values of the NȮ in the aqueous phases of the RMs. We define the NȮ radical (in a RM) system as a π-electron system; m π electrons and n core atoms; $m + n$ = N. The charge and position vector of the j^{th} particle in this system are e_j and r_j, ρ_r^{π} is the π-electron density, and $Q_{CH}^{H}$is σ-π parameter. The hyperfine splitting value, a_r^H, for hydrogen-bonded carbon atom (r^{th} carbon atom) of the 16-DSA is:

$$a_r^H = Q_{CH}^H\rho_r^{\pi} \text{ and } \rho_r^{\pi} = c_{kr}^2 \quad \text{..... (4)}$$

The term c_{kr}^2 relates to the energy level of j^{th} particle as:

$$\phi_k = \sum_{r=1}^{n} c_{kr}\chi_r \quad \text{..... (5)}$$

where, χ_r is the r^{th} atomic orbital. The energy levels of the N particles system a_r^H is: $W = -\sum_{j=1}^{N} e_j r_j$R, where R is the electric field of the RM aqueous phase, and as per the counter ions density levels in the R2 and R3 regions, and the charge density (surfactant head groups) levels in the R2 region. If NȮ radicals reside in a spherical RM having an isotropic solvent (relative permittivity ε_r) with a point dipole at the core as p_r, the Block Walker reaction field R$_R$[16] for NȮ is:

$$R_R = \left(p_r/{R_{RM}}^3\right)(\varepsilon_{\vec{r}}) \quad \text{..... (6)}$$

The reaction field R_R is stronger as the RM size (R$_{RM}$) decreases, indicating that the R_R is stronger with an increase in the head group charge density levels. As the R_R depends on the head group and the counter ions densities in the RMs, the R_R values (as a_N value) exemplify the $\psi(\vec{r})$ acting on the NȮ radicals. We determined the a_N values for RMs of different sizes. The changes in the micro-polarity of the $\vec{r}$ = 0 - $(R_{RM} - l_B)$ region (bulk water) is negligible as a function of the R$_{RM}$ values (ω_0 levels).[8,16] Thus, the a_N values vary as per the micro-polarity aspects of the R2 region. Therefore, the a_N values, as a function of R$_{RM}$, provide a measure of how a_N would be as a function of $\vec{r}$ for a RM. We developed the 'a_N *vs.* ω_0' correlation, which is representative of the a_N *vs.* $\vec{r}$ for the SDS RMs.

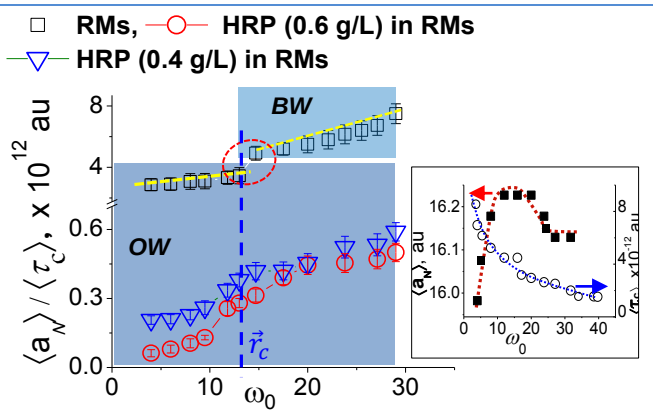

Fig. 2. Assessment of MPA($\vec{r}$) as a function of surfactant-packing: $\langle a_N \rangle/\langle \tau \rangle$ vs. ω_0 ($\vec{r}$). The inset shows $\langle a_N \rangle$ vs. ω_0 ($\vec{r}$) and $\langle \tau \rangle$ vs. ω_0 ($\vec{r}$) relationships. OW and BW represent ordered water and bulk water respectively. The critical distance $\vec{r}_c$ for RMs (without HRP) demarcates (blue line) the OW region from the BW region.

Due to the non-polarity attribute of the R1 region, the a_N values for this region is negligible in comparison to that for the R2 and R3 regions. The rotational coefficient τ_c is particularly pronounced for the non-polar R1 region. Thus, the changes in the a_N for the R1 region, and the τ_c for R2 and R3 regions, as a function of ω_0, are negligible. The a_N and τ_c values can be accounted as:

$$\langle \Delta\tau_c \rangle = p_1\langle \Delta\tau_c \rangle + p_{2+3}\langle \Delta\tau_c \rangle \approx p_1\langle \Delta\tau_c \rangle \quad \text{..... (7)}$$

$$\langle \Delta a_N \rangle = p_1\langle \Delta a_N \rangle + p_{2+3}\langle \Delta a_N \rangle \approx p_{2+3}\langle \Delta a_N \rangle \quad \text{..... (8)}$$

where p_1, p_2 and p_3 are fractional contributions of the regions R1, R2 and R3 respectively.

The $\langle a_N \rangle$ *vs.* ω_0 ($\vec{r}$) profile was considered to assess the MPA($\vec{r}$) of a RM of a particular size.[17] Fig 2 (inset) shows that this profile exhibits a maxima. The lower $\langle a_N \rangle$ values are observed as $\vec{r} \rightarrow$ R$_{RM}$ (interface) and $\vec{r} \rightarrow$ 0 (core). The lower $\langle a_N \rangle$ value at $\omega_0 \approx 5$ level justifies highly ordered forms of water in the R2 region, and presumably due to the relative population of the head groups and the counter ions across the interfacial region being significantly higher. Across the $5 < \omega_0 < 10$ range, the $\langle a_N \rangle$ values are higher with ω_0, which is due to the increase in the volume of the R2 region having less ordered forms of water (in comparison to the highly ordered region at $\omega_0 \approx 5$). The drop in the $\langle a_N \rangle$ *vs.* $\vec{r}$ profile beyond the maxima, at the $\omega_0 > 10$ levels, owe to the increase in the bulk-type water content of the R3 region. At $\omega_0 >> 10$ levels, the bulk water content is higher,, and the plateau region of the $\langle a_N \rangle$ *vs.* $\vec{r}$ profile mostly accounts for the micro-polarity of the bulk-type water in the R3 region. Though these inferences that are made from the $\langle a_N \rangle$ *vs.* $\vec{r}(\omega_0)$ profile provide an assessment of the MPA($\vec{r}$), these inferences are based on the assumption that: the surfactant charge density levels in the SASSs, as per ω_0 levels, exhibit a linear relationship. The surfactant density levels, according to Debye-Stokes-Einstein equation is as:

$$\tau_c = \frac{4\pi\eta(nNV_{chain})}{3kT} \quad \text{..... (9)}$$

Where, η indicates micro-viscosity (inter-surfactant distances), NV_{chain} is the volume of the surfactant chains, and k and T represents Boltzmann constant and temperature, respectively. As the surfactant density level (NV_{chain}) decreases proportionately with increase in the ω_0 values, the corresponding τ_c value would be expected to decrease in a linear fashion. Conversely, Fig 2 (inset) shows that the $\langle \tau_c \rangle$ value decreases in a non-linear fashion (exponentially) as the ω_0 value

Soft Matter Accepted Manuscript

This journal is © The Royal Society of Chemistry 2012

increases. This non-linearity confirms that the inter-surfactant distances (as η) in the SASSs vary with the ω_0 levels. This non-linearity can be justified as that the surfactant content required to stabilize a certain volume of RM water need not be same, e.g., the RM shapes could be slightly different. The studies on RM systems, using small angle x-Ray scattering, small angle neutron scattering and nuclear magnetic resonance techniques, have revealed that the packing-parameter of a surfactant relies on the effective oil-water interfacial area occupied by the surfactant head-group, which is specific according to the volume of RM water.[18] Wherein, an increase in the polar volume for RM system induces a slight increase in the interfacial area and the volume of RM aqueous phase, which altogether justifies the non-linearity observed as a function of w_0 levels. Accordingly, as per the packing aspects of SASSs and, the charge density levels, the point dipole moment p_r and the counter ions distribution (ξ) would vary. As the $\langle a_N \rangle$ value for a ω_0 level could differ based on the SASS packing attributes, the $\langle a_N \rangle$ *vs.* ω_0 profile fails to provide a reliable estimate of the MPA($\vec{r}$). We considered a normalized value of $\langle a_N \rangle$ as $\langle a_N \rangle / \langle \tau_c \rangle$, which accounts for the variability associated with the degree of surfactant-packing in the SASSs for different ω_0 levels.

The $\langle a_N \rangle / \langle \tau_c \rangle$ *vs.* $\vec{r}$ (ω_0) profile was examined to study the MPA($\vec{r}$). The slopes of this profile, $(\Delta(\langle a_N \rangle / \langle \tau_c \rangle)/\Delta \vec{r}$, provide a direct estimate of how the MPA($\vec{r}$) vary as per the differences in the packing attributes of the SASSs. The slope value was higher at the $\omega_0 > 15$ levels, than that at the $\omega_0 < 10$ levels (Fig. 2, dotted lines). At the $\omega_0 < 10$ levels, the lower slope value owes to the ordered form of water in the R2 region, which could be interpreted from the $\langle a_N \rangle$ *vs.* $\vec{r}$ (ω_0) profile as well (Fig.2 (inset)). At $\omega_0 > 15$ levels, $R_{RM} >> l_B$, the higher slope value is due to the plateau region of the $\psi(\vec{r})$ profile that represents the bulk water in the region $|\vec{r}| \leq 0$ - (R-l_B). Instead of the plateau region, as seen in the $\langle a_N \rangle$ *vs.* $\vec{r}$ (ω_0) profile, a higher slope value is seen for the $\langle a_N \rangle / \langle \tau_c \rangle$ *vs.* $\vec{r}$ (ω_0) profile as the τ_c decreases with increase in the ω_0 - decrease in the SASS volume. A non-linearity in the $\langle a_N \rangle / \langle \tau_c \rangle$ *vs.* $\vec{r}$ (ω_0) profile - the deviation shown in a circle in Fig. 2 – demonstrates that the aqueous phase constitutes two spatially segregated regions, having markedly different micro-polarity behaviour. This non-linearity in the $\langle a_N \rangle / \langle \tau_c \rangle$ *vs.* $\vec{r}$ (ω_0) profile is pronounced at a critical distance, $\vec{r_c}$, and demarcates the two regions of a RM. Such a demarcation is the maxima (Fig.2 (inset)) in the $\langle a_N \rangle$ *vs.* $\vec{r}$ (ω_0) profile; the degree of surfactant packing in SASSs is not considered in making this demarcation. Thus, the $\langle a_N \rangle / \langle \tau_c \rangle$ *vs.* $\vec{r}$ (ω_0) profile allows to reliably demarcate the two spatially separable R2 and R3 regions for SDS-hexane RMs, $|\vec{r_c}| = \left(\sqrt{3\omega_0/4\pi}\right)$, $\omega_0 \approx 12$. Though, here, the slope values were similar across the $\omega_0 < 10$ and $\omega_0 > 15$ ranges, it could well be possible that the slope values could vary significantly due to marked differences in the SASS packing aspects.[10]

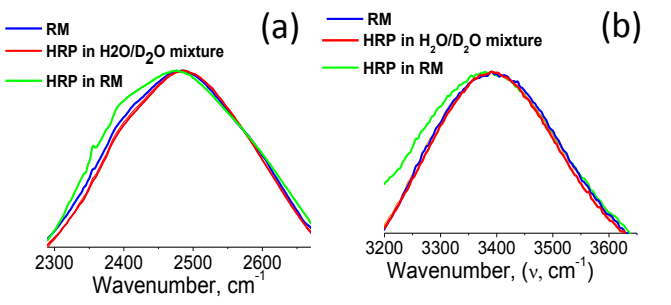

Fig. 3. ATR-FTIR spectra of stretching vibrations of OD (a) and OH (b) stretching vibrations of D_2O and H_2O in RMs, and in presence of HRP. The blue shift of the spectrum (green color sprectral lines) indicate ordered microstructure of the aqueous phase in RM.

The $\langle a_N \rangle / \langle \tau_c \rangle$ *vs.* $\vec{r}$ profiles were developed for the RMs (ω_0 levels) having HRP enzymes at different concentration levels. In comparison to the $\langle a_N \rangle / \langle \tau_c \rangle$ values for the RMs alone, the $\langle a_N \rangle / \langle \tau_c \rangle$ values were significantly lower for RMs having HRP enzymes (Fig. 2). The lower values of $\langle a_N \rangle / \langle \tau_c \rangle$ owe to the HRP-concentration dependent micro-polarity attributes. The differences in the slope values were almost an order of magnitude less with HRP in the RMs (Fig. 2), which strongly suggested that the RM water exhibits ordered form not only in the R2 region but in the R3 region as well. Wherein, the bulk-type water is in negligible amounts in RMs having HRP enzymes. In order to examine the microstructural aspects of the ordered form of water, we studied the O-H/O-D stretching vibration spectroscopic (ATR-IR) absorbance line shapes. In terms of the HRP structural dynamics, there were significant conformational changes of the HRP enzymes in the RMs (ESI 4). The amide I peak of HRP in RMs shifted to lower frequencies, and suggested the transformation of the α-helix structures of HRP to β-sheet types. Based on the negligible changes in the Amide III peak positions and shapes, the possibilities of HRP denaturation in the RMs were eliminated. In terms of the microstructural features of water, for RM of $\omega_0 \approx 20$ level, the blue shifts of the OD- and OH-bands positions (Fig. 3a and b) were prominent for RMs with HRP. These shifts confirmed the ordered forms of water in the R2 and R3 regions. This ordered forms of water could be ascribed to the $\langle a_N \rangle / \langle \tau_c \rangle$ values. In the cases where other shapes of RM are possible and, depending whether the RMs coalesce, the slope values are likely to be different. It would be interesting to see how the $\langle a_N \rangle / \langle \tau_c \rangle$ *vs.* $\vec{r}$ (ω_0) profile could be applicable for RM-enzyme systems to study the dependency of MPA($\vec{r}$) on the surfactant-packing in SASS with surfactants of different chemistries.

ACKNOWLEDGEMENTS

Support from NSF I/UCR Center for Particulate and Surfactant Systems is acknowledged. The authors are thankful to Dr. William Rice at New York Structural Biology Center for the Cryo-SEM studies and Dr. Jun Wu for Analytical Ultra centrifuge studies.

Notes and references

[a] National and Local United Engineering Laboratory for New Petrochemical Materials and Fine Utilization of Resources, Key Laboratory of Resource Fine-Processing and Advanced Materials of Hunan Province and Key Laboratory of Chemical Biology and Traditional Chinese Medicine Research (Ministry of Education of China), College of Chemistry and Chemical Engineering, Hunan Normal University, Changsha, 410081, PR China

[b] College of Environmental Science and Engineering, Hunan University, Changsha 410082, PR China

[c] Langmuir Center for Colloid and Interface Science, Columbia University, New York, 10027, USA

*Corresponding Author: Partha Patra, pp2295@columbia.edu.

REFERNCES

1 Eastoe, J., Hollamby, M. J. & Hudson, L. Recent advances in nanoparticle synthesis with reversed micelles. *Adv Colloid Interfac* **128**, 5-15, doi:DOI 10.1016/j.cis.2006.11.009 (2006).

2 Dekker, M. *et al.* Enzyme Recovery by Liquid-Liquid-Extraction Using Reversed Micelles. *Chem Eng J Bioch Eng* **33**, B27-B33, doi:Doi 10.1016/0300-9467(86)80050-8 (1986).

3 Luisi, P. L. Enzymes Hosted in Reverse Micelles in Hydrocarbon Solution. *Angew Chem Int Edit* **24**, 439-450, doi:DOI 10.1002/anie.198504393 (1985).

4 Dasgupta, A., Das, D. & Das, P. K. Reactivity of trypsin in reverse micelles: neglected role of aggregate size compared to water-pool components. *Biochimie* **87**, 1111-1119, doi:10.1016/j.biochi.2005.05.006 (2005).

5 Melo, E. P., Aires-Barros, M. R. & Cabral, J. M. Reverse micelles and protein biotechnology. *Biotechnology annual review* **7**, 87-129 (2001).

Soft Matter Accepted Manuscript

6 Moilanen, D. E., Fenn, E. E., Wong, D. & Fayer, M. D. Water dynamics in large and small reverse micelles: From two ensembles to collective behavior. *J Chem Phys* **131**, doi:Artn 014704 Doi 10.1063/1.3159779 (2009).
7 Bratko, D., Luzar, A. & Chen, S. H. Electrostatic Model for Protein Reverse Micelle Complexation. *J Chem Phys* **89**, 545-550, doi:Doi 10.1063/1.455443 (1988).
8 Akoum, F. & Parodi, O. Electrostatic Interactions inside the Aqueous Core of Spherical Reversed Micelles (L2-Phase). *J Phys-Paris* **46**, 1675-1681, doi:DOI 10.1051/jphys:0198500460100167500 (1985).
9 Biswas, R., Furtado, J. & Bagchi, B. Layerwise decomposition of water dynamics in reverse micelles: A simulation study of two-dimensional infrared spectrum. *J Chem Phys* **139**, doi:Artn 144906 Doi 10.1063/1.4824446 (2013).
10 Vacha, R., Jungwirth, P., Roke, S. & Frenkel, D. Sodium dodecyl sulfate at water/hydrophobic interfaces. *Abstr Pap Am Chem S* **242** (2011).
11 Vacha, R. *et al.* The Orientation and Charge of Water at the Hydrophobic Oil Droplet-Water Interface. *J Am Chem Soc* **133**, 10204-10210, doi:Doi 10.1021/Ja202081x (2011).
12 Das, D., Roy, S., Mitra, R. N., Dasgupta, A. & Das, P. K. Head-group size or hydrophilicity of surfactants: the major regulator of lipase activity in cationic water-in-oil microemulsions. *Chemistry* **11**, 4881-4889, doi:10.1002/chem.200500244 (2005).
13 Dasgupta, A., Das, D., Mitra, R. N. & Das, P. K. Surfactant tail length-dependent lipase activity profile in cationic water-in-oil microemulsions. *Journal of colloid and interface science* **289**, 566-573, doi:10.1016/j.jcis.2005.03.083 (2005).
14 Kurad, D., Jeschke, G. & Marsh, D. Lipid membrane polarity profiles by high-field EPR. *Biophys J* **85**, 1025-1033, doi:Doi 10.1016/S0006-3495(03)74541-X (2003).
15 Creagh, A. L., Prausnitz, J. M. & Blanch, H. W. Structural and Catalytic Properties of Enzymes in Reverse Micelles. *Enzyme Microb Tech* **15**, 383-392, doi:Doi 10.1016/0141-0229(93)90124-K (1993).
16 Block, H. & Walker, S. M. Modification of Onsager Theory for a Dielectric. *Chem Phys Lett* **19**, 363-364, doi:Doi 10.1016/0009-2614(73)80380-X (1973).
17 Caldararu, H., Caragheorgheopol, A., Vasilescu, M., Dragutan, I. & Lemmetyinen, H. Structure of the Polar Core in Reverse Micelles of Nonionic Poly(Oxyethylene) Surfactants, as Studied by Spin-Probe and Fluorescence Probe Techniques. *J Phys Chem-Us* **98**, 5320-5331, doi:Doi 10.1021/J100071a024 (1994).
18 Pileni, M. P. Reverse Micelles as Microreactors. *J Phys Chem-Us* **97**, 6961-6973, doi:Doi 10.1021/J100129a008 (1993).

Soft Matter Accepted Manuscript

 This journal is © The Royal Society of Chemistry 2012

Table of Contents Entry

Assessment of Micro-Polarity Anisotropy as a function of Surfactant Packing in SDS (sodium dodecyl sulphonate)-Hexane Reverse Micelle Systems

Xin Peng[a, b], Xing-Zhong Yuan[b], P. Somasundaran[c] and Partha Patra[c*]

[a]National and Local United Engineering Laboratory for New Petrochemical Materials and Fine Utilization of Resources, Key Laboratory of Resource Fine-Processing and Advanced Materials of Hunan Province and Key Laboratory of Chemical Biology and Traditional Chinese Medicine Research (Ministry of Education of China), College of Chemistry and Chemical Engineering, College of Environmental Science and Engineering, Hunan University, Changsha, 410082, PR China
[b]College of Environmental Science and Engineering, Hunan University, Changsha 410082, PR China
[c]Langmuir Center for Colloid and Interface Science, Columbia University, New York, 10027, USA

*Corresponding Author: Partha Patra, pp2295@columbia.edu; Phone: 3475183052

Graphic

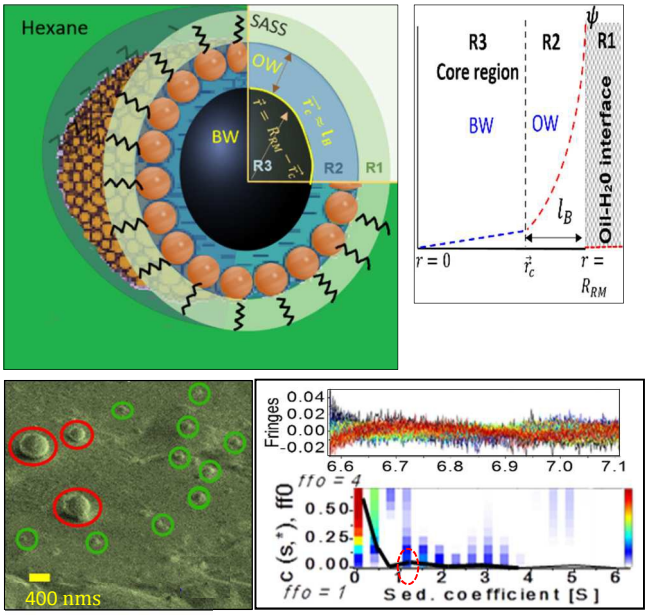

The micro-polarity anisotropy behaviour across the aqueous phase of a SDS (sodium dodecyl sulphonate)-hexane reverse micelle (RM) rely on the SDS packing in the oil-water interfacial self-assembled surfactant structure of the RM.

Soft Matter Accepted Manuscript